ELSEVIER

Materials Science and Engineering A272 (1999) 284–291

MATERIALS SCIENCE & ENGINEERING A

www.elsevier.com/locate/msea

The role of NZP additions in plasma-sprayed YSZ: microstructure, thermal conductivity and phase stability effects

Rodney W. Trice [a], Y. Jennifer Su [a], K.T. Faber [a,*], Hsin Wang [b], Wally Porter [b]

[a] *Department of Materials Science and Engineering, Robert R. McCormick School of Engineering and Applied Science, Northwestern University, Evanston, IL 60208, USA*

[b] *High Temperature Materials Laboratory, Oak Ridge National Laboratory, Oak Ridge, TN 37831, USA*

Received 14 April 1999; received in revised form 14 June 1999

Abstract

A concept for lowering the thermal conductivity of plasma-sprayed yttria-stabilized zirconia (YSZ) was evaluated by adding a low thermal conductivity secondary phase. $Ca_{0.5}Sr_{0.5}Zr_4P_6O_{24}$, a member of the zirconium phosphate or NZP family, was co-sprayed with YSZ using the recently patented small-particle plasma-spray process. The amount of NZP phase in the YSZ varied from 4 to 18 vol.%. Transmission electron microscopy revealed that the plasma-sprayed NZP existed as 30–50 nm size grains when sprayed with YSZ. Between 100 and 1200°C, reductions in the thermal conductivity of NZP/YSZ composite coatings compared to YSZ-only coatings were traced to porosity effects. The NZP phase destabilized the t'-ZrO_2 phase of the YSZ, favoring the formation of t-ZrO_2, then m-ZrO_2, a phase with a high thermal conductivity. Due to this phase change, a large hysteresis was observed in thermal conductivity during the initial heat-up and cool down cycles of the NZP containing samples.

Keywords: Thermal barrier coatings; Zirconium phosphate; Yttria stabilized zirconia; Thermal conductivity

1. Introduction

Thermal barrier coatings (TBCs) offer improved operating efficiencies for gas turbines used in land-based and aircraft-based applications by increasing the operating temperature or decreasing the need for cooling of the metallic structure. A low thermal conductivity coating, typically 7 wt.% Y_2O_3-stabilized ZrO_2, insulates and protects the underlying superalloy from the extreme temperatures and environments experienced during the lifetime of, for example, a combustion liner. With the advent of new, very low thermal conductivity materials, such as the zirconium phosphates (NZP), it may be possible to improve the performance of TBCs by further increasing the operating temperatures of gas turbines (or by reducing the need for cooling).

The family of NZP materials was first systematically evaluated approximately 15 years ago by Roy and co-workers [1,2] demonstrating their extremely low coefficients of thermal expansion (CTE). The CTE can be tailored by ionic substitution of Na, Ca, Sr, Ba, Mg, Cd and other group IA and IIA atoms into NZP's crystal structure [3–5]. Their low CTEs make them attractive as protective coatings for silicon-based ceramics [6] and carbon–carbon composites [7], as well as inserts in diesel engines [8]. NZP has a thermal conductivity, k_{NZP}, of approximately 0.8–1 W/mK for 90% dense materials [8], compared to thermal conductivity of 2–3 W/mK for 90–100% dense yttria-stabilized zirconia [9]. Thus, NZP would seem to be an excellent candidate for thermal protection of superalloys, if not for the large CTE difference between the NZP (approximately 1–2 ppm/°C) and the underlying superalloy (approximately 12 ppm/°C).

Lee et al. [10] noted recently that TBCs are structurally and functionally complex and should be considered as a material system rather than as individual materials. This idea has led to a functionally graded materials approach, combining materials to tailor and exploit the best properties of each constituent. This

* Corresponding author. Tel.: +1-847-491-3537; fax: +1-847-491-7820.

E-mail address: k-faber@nwu.edu (K.T. Faber)

0921-5093/99/$ - see front matter
PII: S0921-5093(99)00468-2

approach has been used in the current research, in which NZP/YSZ composite coatings have been co-sprayed to take advantage of the intrinsic properties of each material. From the NZP additions, low thermal conductivity, low modulus [11], and possibly low oxygen diffusivity are expected [6]. The YSZ matrix provides the high CTE required to match the superalloy, minimizing thermal stresses. Based on previous work [6], a thin dense layer of α-Al_2O_3 would be required to separate the NZP from the MCrAlY bondcoat.

The concept for lowering the thermal conductivity of YSZ coatings involves adding NZP as illustrated in Fig. 1. The equation governing the reduction in the thermal conductivity of the composite coating, k_{Comp}, is as follows [12]:

$$k_{Comp} = k_{YSZ}\frac{1 + 2V_{NZP}\left(\frac{1-k'}{2k'+1}\right)}{1 - V_{NZP}\left(\frac{1-k'}{k'+1}\right)} \quad (1)$$

where V_{NZP} is the volume fraction of NZP, k_{YSZ} is the thermal conductivity of YSZ, and k' is k_{YSZ} divided by k_{NZP}. For plasma-sprayed materials the thermal conductivity is less than that of a sintered material due to the inherent porosity and microcracking within the coating. So, if we assume a k_{NZP} of 0.5 W/mK [13] and k_{YSZ} of approximately 1.0 W/mK [10], then a 17% reduction in k_{Comp} would be expected with 25 vol.% additions of NZP.

In the work being reported, NZP was co-sprayed with YSZ to produce five different composite coatings, with NZP additions varying between 4 and 18 vol.%. Thermal conductivity measurements made on composite coatings were compared to YSZ-only coatings of different densities. The high temperature stability between the NZP and YSZ was evaluated after a 10-hour heat treatment at 1150°C in air. X-Ray diffraction and transmission electron microscopy were used to link the thermal conductivity to the microstructure of the coatings.

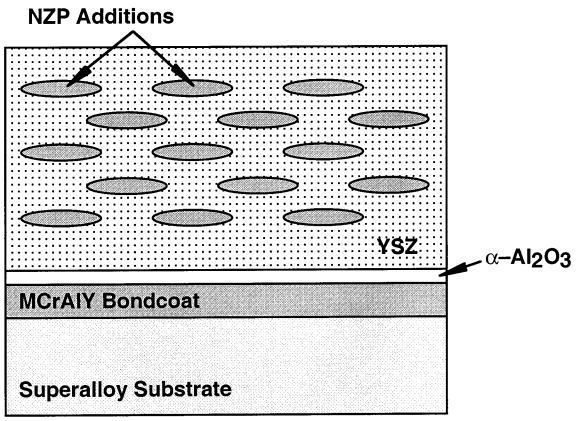

Fig. 1. Idealized schematic of low thermal conductivity phase (NZP) additions to YSZ.

2. Experimental methods and materials

2.1. Materials and the plasma-spray process

A fused and crushed 7 wt.% Y_2O_3–ZrO_2 powder[1] (YSZ), nominally 10 μm in diameter, was used in the current study. It was co-sprayed with $Ca_{0.5}Sr_{0.5}Zr_4P_6O_{24}$[2], an NZP compound with ionic substitution of Ca and Sr atoms. It was a spray-dried powder with an approximate diameter of 50 μm. This particular composition will be referred to simply as NZP hereafter.

All coatings were sprayed using the small-particle plasma-spray (SPPS) process at Northwestern University. SPPS is a recently patented process [14] that allows very small particles to be plasma-sprayed via a specially designed injector [15]. An A-3000 Plasma Technik control system with an F4 gun, mounted on a seven-axis ASEA Brown and Boveri IRB 2000 robot, was used to spray the coatings.

Each powder was fed into the plasma flame through its own externally mounted SPPS injector using a dual disc feeder. The disk speed feeding the YSZ powder was held at a constant speed, varying the disk speed of the NZP powder from zero through 80% of the YSZ disk speed to control the amount of NZP added to the coating. The argon carrier gas that fed the YSZ and NZP powders was held constant at 9 and 5 standard liters per min (slm), respectively. A power of 35 kW with a plasma gas of Ar (at 40 slm) and H_2 (at 10 slm) was used. The spray distance, measured from the injector, was 6 cm. The YSZ and NZP injectors were placed 9 and 10 mm, respectively, from the centerline of the flame. Cooling air was blown on the front and back of the substrates. The speed of the torch rastering across the substrates was 350 mm/s with a 3-mm drop between passes.

All coatings were sprayed on 1018 steel substrates that were initially plasma-spray coated with aluminum. The Al layer facilitated removal of the coating as a weak HCl solution will preferentially attack the aluminum, separating the coating from the substrate. A 220 grit alumina powder was used to gritblast the polished aluminum coating prior to application of the ceramic coatings. Two different YSZ coatings were investigated, including a high (YSZ-H) and a low (YSZ-L) density YSZ coating, with density adjusted by changing the spray parameters. Five co-sprayed coatings were investigated including 5NZP, 10NZP, 15NZP, 25NZP and 30NZP, where, for example, 5NZP signifies that 5 vol.% of NZP was desired to be mixed with the YSZ.

[1] Amperit 825.0, H.C. Starck, Newton, MA.
[2] CS-50, LoTEC Inc., Salt Lake City, UT.

2.2. Physical property measurements and TEM foil preparation

The bulk density of the coatings was measured using the immersion technique. The vol.% of NZP was determined using the point-grid method on polished samples of each coating viewed in a SEM in back-scattered imaging mode. Three different areas were analyzed and averaged for each coating. The theoretical density for each composite coating was calculated using the rule of mixtures with densities for YSZ [16] and NZP [17] assumed to be approximately 6.08 and 3.27 g/cm^3, respectively. The total porosity was calculated using the measured and theoretical densities for each coating.

X-Ray diffraction measurements, using Cu Kα radiation, were made on pulverized coatings of pure YSZ and the NZP/YSZ coatings using a Rigaku Geigerflex Diffractometer to qualitatively determine the phases present after plasma-spray. When required, pure silicon powder was added to the sample to determine any diffraction angle offset associated with sample height, gun alignment, etc.

Cross-sections of 30NZP were thinned by wedge polishing[3], followed by precision ion polishing[4] for about a half-hour, thinning both sides simultaneously. The sample was mounted on a copper grid between the two thinning processes. Two specimen conditions, as-sprayed and 10 h at 1150°C, were evaluated. They were viewed in either a Hitachi HF2000 cFEG or H-8100 transmission electron microscope.

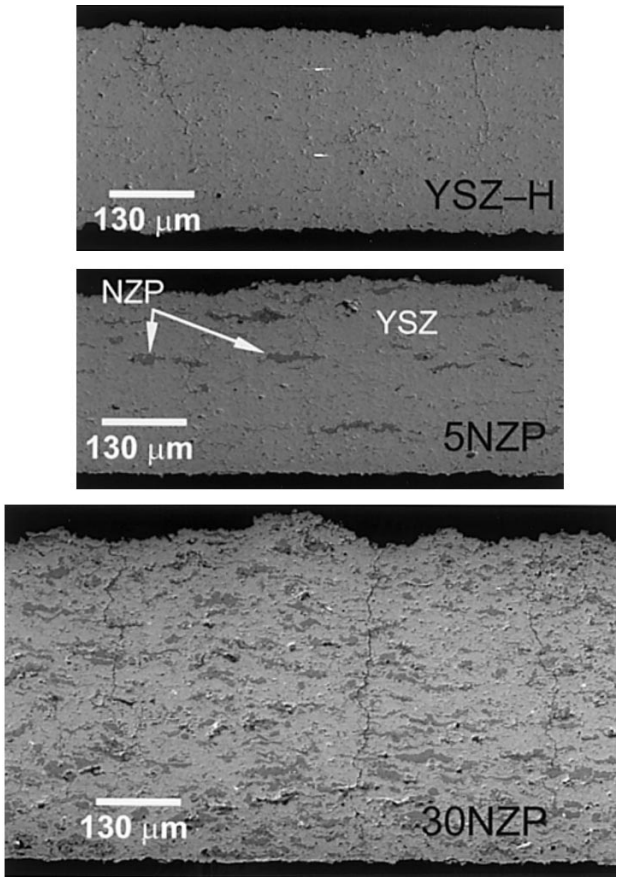

Fig. 2. Typical SEM micrographs from several of the coatings investigated revealing both NZP and YSZ areas.

2.3. Thermal conductivity measurements

A detailed description of the laser flash technique used to determine thermal diffusivity has been published previously [18]. All measurements were made at the High Temperature Materials Laboratory at the Oak Ridge National Laboratory. A disk-shaped sample, 12.5 mm in diameter with a thickness varying from 160 to 500 μm, was used for all tests. Thermal diffusivity was measured between 25 and 1200°C, with some measurements taken during cooling. The time–temperature curves were analyzed by the method of Clark and Taylor [19], which takes into account radiation losses and uses the heating part of the curve to calculate thermal diffusivity. The samples were tested in argon in two furnaces, one for measurements from 25 through 500°C, and another for measurements from 600 through 1200°C. The IR detector was also changed from an InSb detector to a Si detector between 500 and 600°C. Three measurements were taken for each sample at each temperature and averaged. In most cases, two samples of each coating were tested. Samples were tested in sets of six, spending approximately 20–30 min at each temperature.

The specific heat was determined from 100 through 1050°C for each coating with a differential scanning calorimeter[5] using sapphire as the reference standard. The heat-up rate was 20°C/min in an atmosphere of argon. Samples were composed of 4-mm disks, stacked to achieve a mass of approximately 90 mg. Some samples exhibited an exothermic peak in heat flow near 900°C. As a result, samples were given a 1 h heat treatment through 1000°C prior to testing.

The temperature specific thermal diffusivity and specific heat measurements were used to calculate the thermal conductivity according to $k = 100\alpha c_p \rho$ where α is the thermal diffusivity in cm^2/s, c_p is the specific heat in J/g per °C, and ρ is the density in g/cm^3. Specific heat values at 1100 and 1200°C were estimated from a best fit line to the data collected from 100 through 1050°C. Density was assumed constant for the current measurements. The total error associated with each thermal conductivity value is $\pm 6\%$.

[3] South Bay Technology, San Clemente, CA.
[4] Gatan, Model # 691.
[5] Omnitherm DSC 1500.

Table 1
Physical properties measured for the seven coatings investigated

Coating	Desired NZP (vol.%)	Measured NZP (vol.%)	Density (g/cm^3)	Theoretical density (g/cm^3)	% Dense	Total porosity (%)
YSZ-H	0	0	5.36	6.08	88.2	11.8
YSZ-L	0	0	5.02	6.08	82.6	17.4
5NZP	5	3.9 ± 1.9	5.19	5.97*	86.9	13.1
10NZP	10	8.2 ± 0.6	4.91	5.85*	83.9	16.1
15NZP	15	11.5 ± 0.8	4.73	5.76*	82.1	17.9
25NZP	25	17.8 ± 1.0	4.59	5.58*	82.3	17.7
30NZP	30	16.7 ± 1.1	4.61	5.61*	82.2	17.8

* Based on a rule of mixtures calculation, assuming theoretical densities of 6.08 and 3.27 g/cm^3 for YSZ and NZP, respectively.

3. Results and discussion

3.1. Microstructure of As-sprayed NZP/YSZ coatings

Fig. 2 shows polished SEM cross-sections of several of the coatings presently studied. As tunnel cracks were apparent in both of the YSZ-only coatings, tunnel cracks observed in the NZP/YSZ coatings are likely due to the YSZ phase. The NZP primarily existed as large 50- to 100-μm long globules in the YSZ. This morphology was likely a result of the large starting size of the NZP powder relative to the YSZ powder. No cracking was observed in the globules of NZP when viewed at higher magnifications, consistent with previous observations for dense samples of $Ca_{0.5}Sr_{0.5}Zr_4P_6O_{24}$ [4].

Table 1 presents the desired and actual amount of NZP observed in the coatings. The actual amount of NZP ranged from 4 to 18 vol.%. For NZP loadings greater than 11 vol.%, approximately 17–18 vol.% porosity was observed in the NZP/YSZ coatings. The porosity in the YSZ coatings varied from 11.8 to 17.4 vol.% for YSZ-H and YSZ-L, respectively. Fig. 3 shows the X-ray diffraction data obtained on a typical as-sprayed composite coating (30NZP), with only YSZ (t'-phase) and NZP observed.

A bright field TEM micrograph of 30NZP is shown in Fig. 4a, with the NZP and YSZ phases identified using EDS. Individual lamellae with columnar grains were observed for YSZ. The NZP phase did not exhibit typical lamellar morphology, but rather, remained nanocrystalline with grains estimated at 30–50 nm in diameter. Fig. 4b is a selected area diffraction micrograph from the NZP region indicating small grains. Nanocrystalline grains have been observed before in plasma-sprayed YSZ, but only in isolated areas [20], with its microstructure attributed to homogenous nucleation. In 30NZP all regions of NZP investigated were nanocrystalline. However, grain sizes in the 30- to 50-nm diameter range are not expected to decrease the thermal conductivity [9]. Further inspection of Fig. 4a reveals complete filling of the regions between YSZ lamellae with NZP, indicating complete melting during plasma spraying.

3.2. Thermal conductivity results (initial heat-up)

The thermal conductivity results generated during the initial heat-up of the samples from the seven coatings are shown in Fig. 5. The data shift between 500 and 600°C is an experimental artifact, due to the change from the low temperature furnace to the high temperature furnace. There was a clear decrease in the thermal conductivity of the NZP/YSZ and YSZ-L coatings over the YSZ-H coating. This was most evident for 25NZP and 30NZP, with a 25% reduction in thermal conductivity compared to $k_{YSZ\text{-}H}$ at some temperatures. A steady increase in the thermal conductivity was observed from 900 through 1200°C in all coatings.

Fig. 6a and b shows the thermal conductivity of each coating plotted versus the percent density at 500 and 1000°C, respectively. The percent density was defined as the measured bulk density divided by the defect-free density (or theoretical density) of each coating. A dotted line has been drawn between the thermal conductivities of the high and low density YSZ coatings to establish trends associated with increasing porosity. All

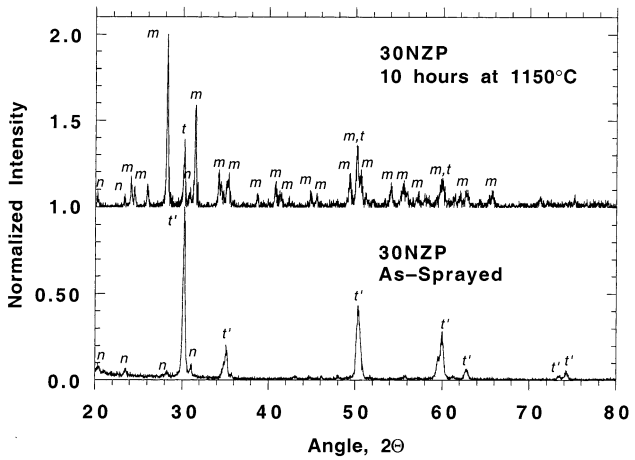

Fig. 3. Comparison of the 30NZP as-sprayed and heat-treated coatings. Monoclinic zirconia is the dominant phase and results from first the decomposition of the t'-ZrO_2 to t-ZrO_2, and second, the final transformation to m-ZrO_2 in the heat-treated sample (n = NZP, m = m-ZrO_2, t = t-ZrO_2, and t′ = t'-ZrO_2).

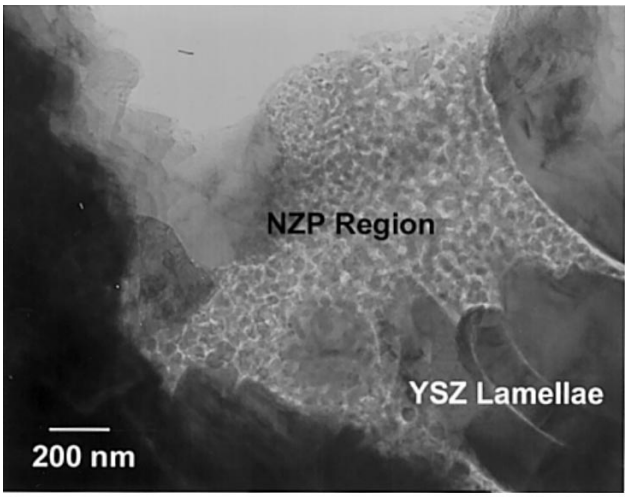

(a)

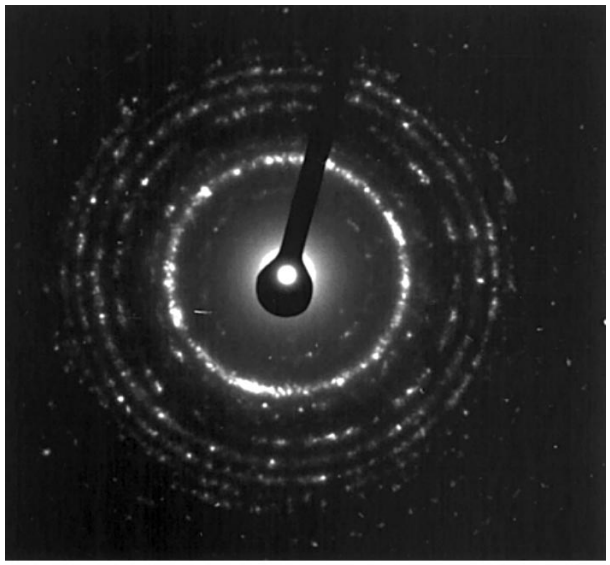

(b)

Fig. 4. (a) Bright field TEM micrograph of 30NZP viewed in cross-section. The YSZ phase exhibited thin lamellae with columnar grains. Small, 30- to 50-nm diameter grains of NZP were observed. (b) Selected area diffraction of the NZP region indicating small grains. No amorphous phase was noted.

reductions in the thermal conductivity of YSZ/NZP composite coatings as compared to YSZ-only coatings were attributed to increasing porosity, and not NZP effects. The reasons for this 'non-effect' are attributed to the microstructure of the NZP phase.

Most of the reduction in the thermal conductivity of plasma-sprayed coatings, as compared to identical materials made via a powder compaction/sintering route, is due to the microstructure of the lamellae that comprise the coating. Extremely fine porosity (approximately 0.1 μm) has been observed between the individual lamellae, resulting in only 20% contact between adjacent lamellae [21,22]. Heat flow through the thickness of the coating is significantly reduced by this micro-porosity. The NZP phase studied presently did not exhibit this morphology, but rather, solidified as a nanocrystalline phase with apparently good contact between the grains (Fig. 4a). Thus, the NZP phase would be expected to have the thermal conductivity associated with a dense NZP material (nearly 1 W/mK) because the microstructural features that reduce its thermal conductivity were not present. As such, no reduction in the thermal conductivity of the NZP/YSZ coating would be expected because the NZP does not exhibit reduced thermal conductivity compared to the YSZ.

3.3. Thermal conductivity results (cool down)

Fig. 7 is a plot of the hysteresis observed in thermal conductivity during the initial heat-up and cool down cycles for YSZ-L and 30NZP. For 30NZP, a 0.6 W/mK increase in thermal conductivity was observed between the heat-up and cool down cycles at 600°C. At the same temperature, YSZ-L demonstrated a difference in thermal conductivity of only 0.3 W/mK. An increase in thermal conductivity of plasma-sprayed YSZ coatings with increasing temperature is expected due to decreasing porosity (via sintering) and microcrack closure across lamellae boundaries [23]. This would increase both the thermal diffusivity and the density of a coating. However, despite being exposed to the same temperature cycles and having the same initial porosity, a distinct difference in thermal conductivity hysteresis was observed between 30NZP and YSZ-L. Thus, an additional mechanism must be operative in 30NZP that results in increased hysteresis. This mechanism can be

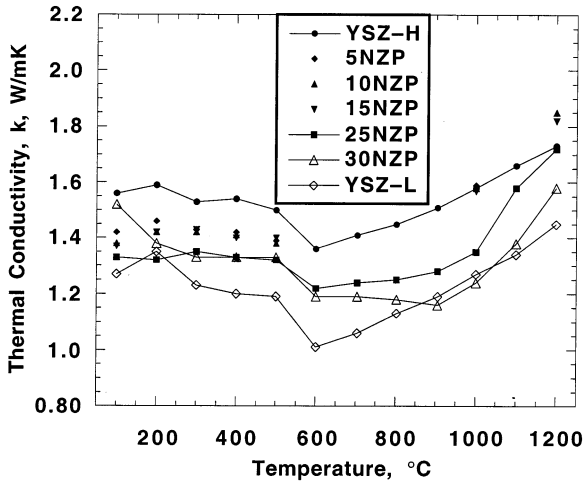

Fig. 5. The thermal conductivity for the seven coatings tested. Lines were drawn through the data to aid the eye. No data were taken for 5NZP, 10NZP or 15NZP between 600 and 900°C. The error associated with the measurements is ±6%.

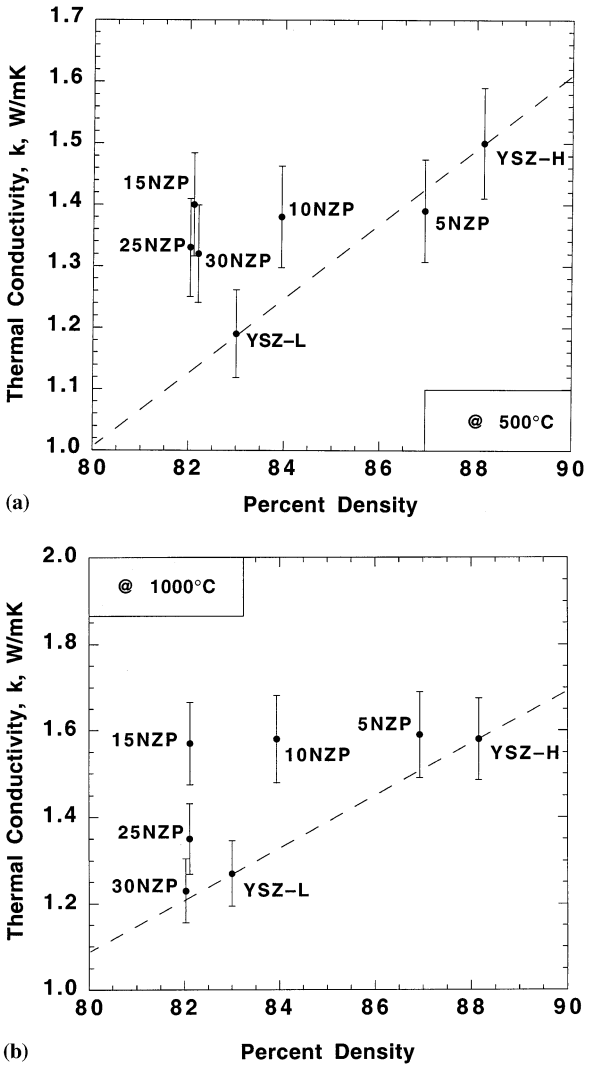

Fig. 6. A plot of thermal conductivity versus percent density from data taken at (a) 500°C and (b) 1000°C. A dotted line has been drawn to connect the YSZ-H and YSZ-L coatings. The apparent reduction in k observed in Fig. 5 for the NZP/YSZ coatings over YSZ-H are primarily due to porosity effects.

traced to microstructural changes in the YSZ caused by the NZP phase.

During plasma-spraying, the melted YSZ undergoes rapid cooling upon impact with the substrate. The result is that metastable tetragonal zirconia (t'-ZrO_2) is formed, containing 7 wt.% yttria, rather than t-ZrO_2, which contains 4 wt.% yttria [24,25]. The t'-ZrO_2 phase is desirable as it decomposes into t-ZrO_2 (and c-ZrO_2) very slowly, ultimately delaying the formation of monoclinic zirconia (m-ZrO_2).

The effect of NZP on the stability of the t'-ZrO_2 phase in YSZ was investigated using the X-ray diffraction analysis of Muraleedharan et al. [24] Fig. 8 compares these results. The t'-ZrO_2 phase of the YSZ was observed in the as-sprayed YSZ-H and 30NZP coatings. The t'-ZrO_2 phase was still evident in YSZ-H after 10 h at 1150°C. However, in 30NZP after an identical heat treatment, neither t- or t'-ZrO_2 was observed. Thus it appears that the NZP phase destabilized the t'-ZrO_2 phase. At an intermediate temperature and a longer heating cycle, 1000°C for 100 h, the YSZ phase in the 30NZP coating was fully converted to t-ZrO_2, the first step in the decomposition of t'-ZrO_2.

A comparison of the 30NZP coating in the as-sprayed condition and after a 10-h heat treatment at 1150°C over a wide range of diffraction angles is shown in Fig. 3. As a result of the heat treatment, m-ZrO_2 has grown at the expense of the tetragonal phase of zirconia. Thus, the end result of destabilization of the t'-ZrO_2 phase (observed in Fig. 8) is that m-ZrO_2 is readily formed. The mechanistic reason for this destabilization may be related to NZP's affinity for yttrium [13], however, this will be addressed in future research.

The m-ZrO_2 phase is undesirable for two reasons. First, polycrystalline monoclinic zirconia has a high thermal conductivity compared to the tetragonal phases [9]. At room temperature, 98% dense m-ZrO_2 has a thermal conductivity of approximately 6.5 W/mK compared to 2.8 W/mK observed for 98% dense t-ZrO_2.

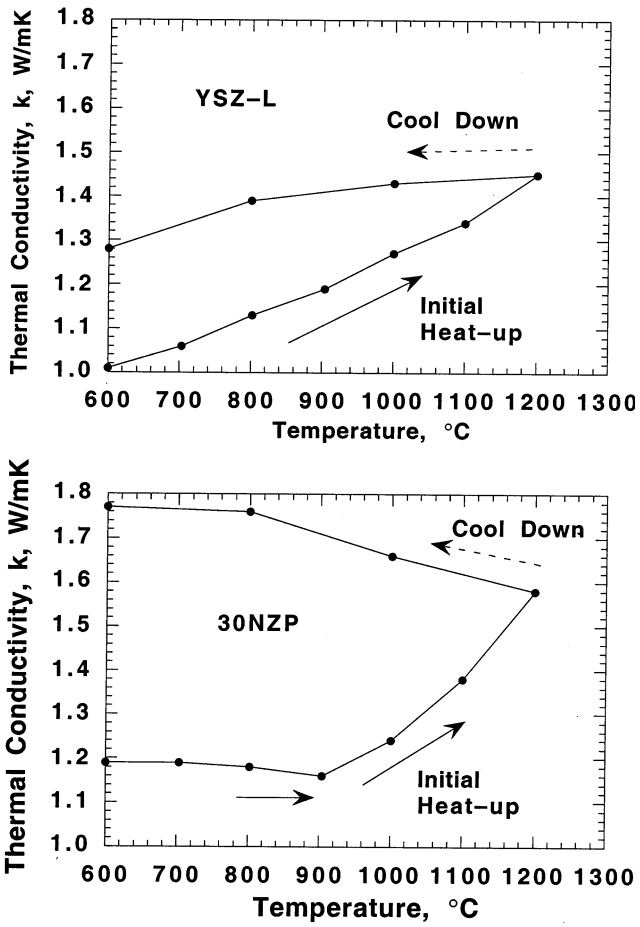

Fig. 7. A plot of the hysteresis observed in thermal conductivity during the initial heat-up and cool down of coating (a) YSZ-L and (b) 30NZP.

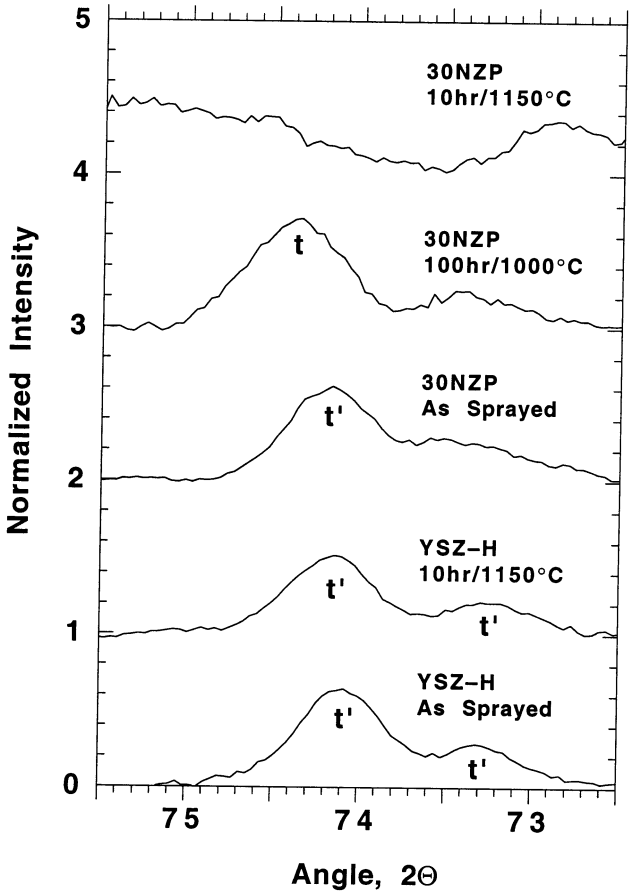

Fig. 8. X-Ray diffraction results reveal that NZP additions decrease the high temperature stability of the t'-ZrO_2 phase. Each set of X-ray data was normalized to its largest peak.

X-Ray investigation of the actual thermal diffusivity samples used for 30NZP revealed the presence of an appreciable amount of the m-ZrO_2 phase. The effect of this phase is apparent in Fig. 7, where a large thermal conductivity hysteresis was observed for NZP containing coatings. Clearly, the destabilization of t'-ZrO_2 to m-ZrO_2 results in increased thermal conductivity of the coating. It is also important to remember that the thermal conductivity of YSZ coatings containing NZP would likely increase until t-ZrO_2 has fully transformed to m-ZrO_2.

The second reason monoclinic zirconia is not desired is related to the 3.5% volume expansion associated with the t- to m-ZrO_2 transformation. While this is often a beneficial transformation when stress-induced [26], the volume increase can lead to microcracking between grains, reducing the mechanical integrity of the coating. Fig. 9 is a bright field TEM micrograph of 30NZP after 10 h at 1150°C. Grain boundary cracking was observed between grains of monoclinic zirconia, a result of the volume increase associated with the phase transformation.

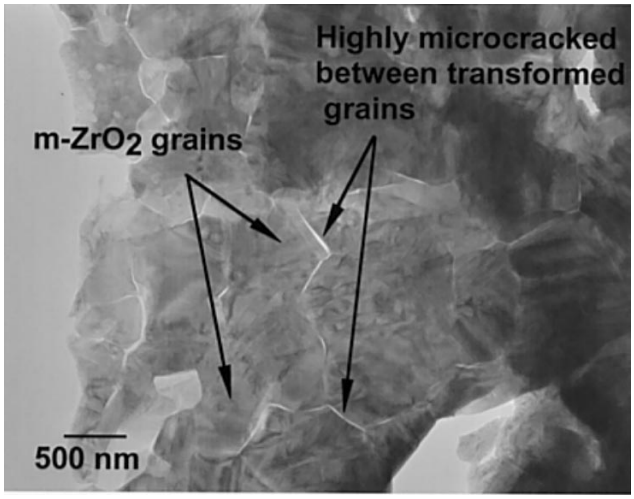

Fig. 9. Bright field TEM micrograph of 30NZP after 10 h at 1150°C. Cracks were observed along the grain boundaries where tetragonal zirconia grains transformed into m-ZrO_2 grains. Note the twinned microstructure in the transformed grains of zirconia. Note the twinned microstructure in the transformed grains of zirconia.

4. Conclusions

A concept for lowering the thermal conductivity of plasma-sprayed yttria-stabilized zirconia was evaluated by adding NZP, a material with a lower thermal conductivity than YSZ. Composite coatings were fabricated by co-spraying the two phases, each with its own powder injector, using small-particle plasma spray. The amount of NZP in these coatings ranged from 4 to 18 vol.%.

No decrease in thermal conductivity was observed after adding NZP to YSZ. This was believed to be due to the microstructure of the NZP, which formed dense regions of nano-sized crystals rather than lamellae. Thus, the microstructural features responsible for lowering the thermal conductivity of plasma-sprayed coatings (microporosity and cracks between lamellae) were not formed in the NZP.

Furthermore, NZP destabilized the t'-ZrO_2 phase, causing t-ZrO_2 to form at temperatures much lower than required for this transformation to occur in YSZ-only coatings. This transformation promoted formation of monoclinic zirconia, a phase with a high thermal conductivity compared to tetragonal zirconia. The structural integrity of the coating was also affected by this transformation, resulting in microcracks between transformed m-ZrO_2 grains.

Acknowledgements

The authors wish to thank Rick Marzec for fabrication of the coatings used in this study, Dr Chiou for assistance with the TEM, and Tom Easley and Luke

Brewer for help in editing the final document. Also, Rama Nageswaran provided valuable insight into NZP. This work was supported by the U.S. Department of Energy, Federal Energy Technology Center, Cooperative Agreement No. DE-FC21-92MC29061, under subcontract 96-01-SR047. The thermal conductivity testing was supported by the U.S. DOE, Assistant Secretary for Energy Efficiency and Renewable Energy, Office of Transportation Technologies, as part of the HTML User Program under contract DE-AC05-96OR22464, managed by Lockheed Martin Energy Research Corporation.

References

[1] J. Alamo, R. Roy, Ultralow expansion ceramics in the system $Na_2O–ZrO_2–SiO_2$, J. Am. Ceram. Soc. 679 (5) (1984) C78–C79.
[2] R. Roy, D.K. Agrawal, J. Alamo, R.A. Roy, [CTP]: A new structural family of near-zero expansion ceramics, Mater. Res. Bull. 19 (2) (1984) 471–477.
[3] S.Y. Limaye, D.K. Agrawal, R. Roy, Y. Mehrotra, Synthesis, sintering and thermal expansion of $Ca_{1-x}Sr_xZr_4P_6O_{24}$—An ultra-low thermal expansion ceramic system, J. Mater. Sci. 26 (1991) 93–98.
[4] V. Srikanth, E.C. Subbarao, D.K. Agrawal, C.-Y. Huang, R. Roy, G.V. Rao, Thermal expansion anisotropy and acoustic emission of $NaZr_2P_3O_{12}$ family ceramics, J. Am. Ceram. Soc. 74 (2) (1991) 365–368.
[5] R. Brochu, M. El-Yacoubi, M. Louer, A. Serghini, M. Alami, D. Louer, Crystal chemistry and thermal expansion of $Cd_{0.5}Zr_2(PO_4)_3$ and $Cd_{0.25}Sr_{0.25}Zr_2(PO_4)_3$ ceramics, Mater. Res. Bull. 32 (1) (1997) 15–23.
[6] W.Y. Lee, K.M. Cooley, C.C. Berndt, D.L. Joslin, D.P. Stinton, High-temperature chemical stability of plasma-sprayed $Ca_{0.5}Sr_{0.5}Zr_4P_6O_{24}$ coatings on Nicalon/SiC ceramic matrix composite and Ni-based superalloy substrates, J. Am. Ceram. Soc. 79 (10) (1996) 2759–2762.
[7] D.K. Agrawal, G. Harshe, E. Breval, R. Roy, [NZP], $NaZr_2P_3O_{12}$-type materials for protection of carbon–carbon composites, J. Mater. Res. 11 (12) (1996) 3158–3163.
[8] S.Y. Limaye, R. Nageswaran, Development of NZP ceramic based cast-in-place diesel engine port liners, Final Report, LoTec, Inc., West Valley City, UT, November 1994.
[9] S. Raghavan, H. Wang, R.B. Dinwiddie, W.D. Porter, M.J. Mayo, The effect of grain size, porosity, and yttria content on the thermal conductivity of nanocrystalline zirconia, Scripta Mater. 38 (8) (1998) 1119–1125.
[10] W.Y. Lee, D.P. Stintion, C.C. Berndt, F. Erdogan, Y.-D. Lee, Z. Mutasim, Concept of functionally graded materials for advanced thermal barrier coating applications, J. Am. Ceram. Soc. 79 (12) (1996) 3003–3012.
[11] G. Harshe, D. Agrawal, High-temperature mechanical properties and chemical stability of $Ba_{1+x}Zr_4P_{6-2x}Si_{2x}O_{24}$ low-thermal-expansion ceramics, J. Am. Ceram. Soc. 77 (7) (1994) 1965–1968.
[12] W.D. Kingery, H.K. Bowman, D.R. Uhlmann, Introduction to Ceramics, Wiley, New York, 1976, p. 636.
[13] Rama Nageswaran, LoTEC Industries, private communication.
[14] T.F. Bernecki, D.R. Marron, Small-particle plasma-spray apparatus, method and coated article, U.S. Patent # 5,744,777.
[15] R.W. Trice, K.T. Faber, The role of particle splashing on the microstructural development and mechanical properties of small-particle plasma-sprayed alumina, J. Am. Ceram. Soc., in press.
[16] J.B. Wachtman, Mechanical Properties of Ceramics, Wiley, New York, 1996, p. 392.
[17] S.Y. Limaye, D.K. Agrawal, H.A. McKinstry, Synthesis and thermal expansion of $MZr_4P_6O_{24}$ (M = Mg, Ca, Sr, Ba), J. Am. Ceram. Soc. 70 (10) (1987) C232–C236.
[18] H. Wang, R.B. Dinwiddie, P.A. Gaal, Multiple station thermal diffusivity instrument, in: K.E. Wilkes, R.B. Dinwiddie, R.S. Graves (Eds.), Thermal Conductivity 23, Technomic Publishing, 1996, pp. 119–127.
[19] L.M. Clark III, R.E. Taylor, Radiation loss in the flash method for thermal diffusivity, J. Appl. Phys. 46 (2) (1975) 714–719.
[20] P.D. Harmsworth, S. Stevens, Microstructure of zirconia–yttria plasma-sprayed thermal barrier coatings, J. Mater. Sci. 27 (1992) 616–624.
[21] R. McPherson, A review of microstructure and properties of plasma-sprayed ceramic coatings, Surface Coatings Technol. 39/40 (1989) 173–181.
[22] A.R. de Arellano-Lopez, K.T. Faber, Microstructural characterization of small-particle plasma-spray coatings, J. Am. Ceram. Soc. 82(8) (1999) 2204–2208.
[23] R. Dutton, R. Wheeler, K.S. Ravichandran, K. An, Effect of heat treatment on the thermal conductivity of plasma-sprayed thermal barrier coatings, J. Therm. Spray Technol, submitted.
[24] K. Muraleedharan, J. Subrahmanyam, S.B. Bhaduri, Identification of t′ phase in ZrO_2–7.5 wt.% Y_2O_3 thermal barrier coatings, J. Am. Ceram. Soc. 71 (5) (1988) C226–C227.
[25] V. Lanteri, R. Chaim, A.H. Heuer, On the microstructures resulting from the diffusionless cubic to tetragonal transformation in ZrO_2–Y_2O_3 alloys, J. Am. Ceram. Soc. 69 (10) (1986) C251–C261.
[26] A.H. Heuer, Transformation toughening in ZrO_2-containing ceramics, J. Am. Ceram. Soc. 70 (10) (1987) 689–698.